The Meteoritical Society

Meteoritics & Planetary Science 1–18 (2026)
doi: 10.1111/maps.70176

Visible, near-, and thermal infrared spectra of asteroid Bennu samples: Relationship to and implications for remote sensing of carbonaceous asteroids

V. E. HAMILTON[1]*, E. A. CLOUTIS[2], R. E. MILLIKEN[3], P. HAENECOUR[4], D. R. GOLISH[4], K. J. DOMANIK[4], T. J. McCOY[5], L. P. KELLER[6], A. A. SIMON[7], H. H. KAPLAN[7], C. A. GOODRICH[8], S. A. SANDFORD[9], D. APPLIN[2], T. HIROI[3], D. H. HILL[4], N. G. LUNNING[6], F. M. McCUBBIN[6], S. A. ECKLEY[10], C. J. SNEAD[6], E. H. BLUMENFELD[10], J. E. AEBERSOLD[11], C. SCHULTZ[3], N. BOWLES[12], K. A. SHIRLEY[12], S. S. RUSSELL[13], J. J. BARNES[4], T. J. ZEGA[4], D. N. DELLAGIUSTINA[4], A. J. RYAN[4], D. P. GLAVIN[7], J. P. DWORKIN[7], H. C. CONNOLLY Jr.[4,14,15], and D. S. LAURETTA[4]

[1]Southwest Research Institute, Boulder, Colorado, USA
[2]Department of Geography, University of Winnipeg, Winnipeg, Manitoba, Canada
[3]Department of Earth, Environmental and Planetary Sciences, Brown University, Providence, Rhode Island, USA
[4]Lunar and Planetary Laboratory, University of Arizona, Tucson, Arizona, USA
[5]Department of Mineral Sciences, National Museum of Natural History, Smithsonian Institution, Washington, DC, USA
[6]ARES (Astromaterials Research & Exploration Science), NASA Johnson Space Center, Houston, Texas, USA
[7]Solar System Exploration Division, NASA Goddard Space Flight Center, Greenbelt, Maryland, USA
[8]Lunar and Planetary Institute, USRA, Houston, Texas, USA
[9]NASA Ames Research Center, Moffett Field, California, USA
[10]Amentum—JETS 2, NASA Johnson Space Center, Houston, Texas, USA
[11]Texas State University, JETS II, Houston, Texas, USA
[12]Department of Physics, Oxford University, Oxford, UK
[13]Planetary Materials Group, Natural History Museum, London, UK
[14]Department of Geology, Rowan University, Glassboro, New Jersey, USA
[15]Department of Earth and Planetary Sciences, American Museum of Natural History, New York, New York, USA

***Correspondence**
V. E. Hamilton, Southwest Research Institute, Boulder, CO, USA.
Email: vicky.hamilton@swri.org

(Received 21 November 2025; revision accepted 18 May 2026)

Abstract–Remote spectroscopy is used to characterize the mineralogy and infer the history of planetary bodies. Carbonaceous asteroids, such as B-type (101955) Bennu, represent the earliest stages of planet formation. B types have a blue (negative) spectral slope and comprise <5% of asteroids. Samples from Bennu returned by the OSIRIS-REx spacecraft complement remote observations of this rare population. We show here, using laboratory spectra that are directly comparable to spacecraft data, that OSIRIS-REx accurately determined Bennu's dust content and most of its surface composition. However, spectra of the asteroid exhibit stronger water absorptions than those of bulk samples, possibly due to hydrous, Mg-rich phosphate or solar wind implantation at Bennu's uppermost surface. Bennu samples spectrally resemble the most aqueously altered carbonaceous meteorites and samples of (162173) Ryugu, indicating similarly pervasive aqueous alteration. However, one carbon-enriched Bennu stone does not appear to have a spectral analog among Ryugu samples or meteorites. Our findings demonstrate the leverage obtained using a wide range of wavelengths and that sample analysis anchors the

interpretations of remote sensing, leading to more robust characterization of planetary surface composition and evolution.

INTRODUCTION

The Origins, Spectral Interpretation, Resource Identification, and Security–Regolith Explorer (OSIRIS-REx) mission (Lauretta et al., 2015) targeted Bennu because its rare B-type spectrum (Clark et al., 2011; DeMeo et al., 2009) suggested that it would comprise primitive, carbonaceous materials that preserve water-bearing minerals and organic compounds formed early in solar system history. Remotely sensed data acquired by the OSIRIS-REx Visible and InfraRed Spectrometer (OVIRS, Reuter et al., 2018) and Thermal Emission Spectrometer (OTES, Christensen et al., 2018) corroborated these expectations and indicated that Bennu is dominated (>80 vol%) by hydrated Mg-phyllosilicate minerals, with lesser magnetite, carbonates, organics, and <10 vol% anhydrous silicates (Hamilton et al., 2019, 2021; Lauretta et al., 2019; Simon, Kaplan, Cloutis, et al., 2020; Simon, Kaplan, Hamilton, et al., 2020)—typical for aqueously altered, primitive carbonaceous materials. Spectral data also indicated small amounts of pyroxene-bearing exogenic material scattered across the asteroid (e.g., DellaGiustina et al., 2021).

Bennu's global visible to near-infrared (VNIR) spectrum is virtually constant in 89% (2σ) of the data (±65° latitude, ~90% surface area) acquired by OVIRS at 12:30 pm local solar time, with the remaining variation attributable to changes in the 1.0–2.5 μm slope (Barucci et al., 2020). The position (2.74 ± 0.01 μm) and area of the colloquial "3 μm" hydration band do not vary substantially (Barucci et al., 2020), though in a study of 45 craters (Deshapriya et al., 2021), 20 exhibited slight shifts in this band's position, for example, −0.015 μm at Hokioi crater, the OSIRIS-REx sampling site. Hokioi is among the reddest craters and darkest locations on the asteroid (Barucci et al., 2020; Deshapriya et al., 2021) and became even redder and darker after sampling (Lauretta et al., 2022; Praet et al., 2022), but no change in the position of the hydration feature was detected (Praet et al., 2022). No changes in 3 μm band depth have been uniquely attributed to H content.

The global-average blue slope is attributed to the end stage of a complex space weathering process, with the most recent exposures exhibiting redder (less blue) slopes (Clark et al., 2023; DellaGiustina et al., 2020; Lauretta et al., 2022). Thermal infrared (TIR) data are dominated by phyllosilicate features (>80 vol%) with magnetite and exhibit two global endmembers, interpreted to represent differences in the thickness and particle sizes (in the low tens of microns in both cases) of minor dust deposits (Hamilton et al., 2021). The distribution of these endmembers loosely corresponds with boulder populations having darker and rougher versus brighter and smoother surfaces (DellaGiustina et al., 2020) that may result in variable trapping of small particles (Hamilton et al., 2021; Jawin et al., 2022). No substantial change was detected in the TIR spectrum of Hokioi crater after sampling (Lauretta et al., 2022).

OSIRIS-REx delivered samples of Bennu to the Earth in September 2023. A major mission objective (Lauretta et al., 2023) is to evaluate, using the samples, whether remote sensing analyses accurately characterized Bennu. Initial laboratory analyses of aggregate material (unsorted particles <0.5 cm) confirmed the presence and abundances of the main predicted phases (Connolly Jr et al., 2025; Lauretta et al., 2024): phyllosilicates comprise >˜80 vol% of the mineralogy, with magnetite constituting ~3–5 vol%, carbonates <˜3–4 vol%, and anhydrous silicates <4 vol%. The dominant solid-solution carbonate composition, dolomite, was also correctly determined (Kaplan et al., 2020; Lauretta et al., 2024). Organic compounds are present as expected (Glavin et al., 2025), as are sulfides, which were not detected remotely but were predicted based on Bennu's closest meteorite analogs (Hamilton et al., 2021).

However, hydrous Mg-rich (formerly referred to as Mg,Na-) phosphates were discovered in the samples (Lauretta et al., 2024), commonly concentrated in veins and on fracture surfaces, which were neither expected from meteorite analogs nor detected remotely. Furthermore, the visible spectral slope of an aggregate sample was red (positive)—more so than any area observed on Bennu (Lauretta et al., 2024). These findings necessitate detailed spectral investigation, not only of aggregate material but also of individual particles, to be understood in the context of the remote data.

Here, we report VNIR spectra of an aggregate Bennu sample, TIR spectra of polished sections from centimeter-scale stones representing three broad categories of Bennu particles—angular, hummocky, and mottled (Lauretta et al., 2024)—with at least the former two representing distinct lithologies (Connolly Jr et al., 2025) and VNIR and TIR spectra of fragments (up to ~5–8 mm) of a mottled stone (Table 1). These data allow us to evaluate comprehensively the accuracy of remote compositional and physical characteristics, place Bennu in context with meteorites and Ryugu, and inform interpretations and future observations of near-Earth asteroids.

TABLE 1. OSIRIS-REx sample and analysis information.

Sample number	Sample type	Laboratory	Measurement	DOI
OREX-800029-0	Unprepared bulk aggregate particles	U. Winnipeg	VNIR	10.60707/qb54-tp08; 10.60707/p2n3-xv14; 10.60707/dyyc-yd79; 10.60707/r6wt-3444; 10.60707/gd9r-8737; 10.60707/qr80-ca24; 10.60707/a81c-2x76
OREX-800029-0	Unprepared bulk aggregate particles	Brown U.	VNIR/TIR	10.60707/pw1a-2296; 10.60707/dqts-2513
OREX-800073-0	Unprepared mottled particles	Brown U.	VNIR/TIR	10.60707/b74w-8b58; 10.60707/m0p4-8s12
OREX-800055-16	Polished section	SwRI	TIR	10.60707/gkqn-cr57
OREX-800088-11	Polished section	SwRI	TIR	10.60707/98x7-bb30
OREX-800023-16	Polished section	SwRI	TIR	10.60707/h5wa-eg65
OREX-800023-16	Polished section	UA	BSE, EMPA	10.60707/pyay-ht62; 10.60707/s213-jb56

Note: Measurements are as follows: visible and near-infrared (VNIR) spectroscopy, thermal infrared (TIR) spectroscopy, backscattered electron image (BSE), electron microprobe analysis (EMPA).

METHODS

Sample Preparation and Supporting Characterization Techniques

The samples measured in this work are listed in Table 1. The bulk aggregate is an unsorted, unprepared sampling of granular particulates, with typical sizes less than several hundred microns, not a "powder" per se. The polished sections were produced at NASA's Johnson Space Center (JSC) using the methods described by Harrington et al. (2025).

The parent stones of all polished sections were characterized by XCT under pristine conditions at JSC (Eckley et al., 2025; Lunning & Davidson, 2025) at a voxel size of 8.00 μm. Mottled stone OREX-800023-0, containing Mg-rich phosphate, had an original mass of 399 mg ± 5 mg. To determine the volumetric abundance of Mg-rich phosphate in this stone, we applied machine learning techniques to the XCT data. These phosphates have very low x-ray attenuation, approaching the level of ambient air, complicating typical grayscale threshold-based segmentation methods for mapping. Deep learning tools in Dragonfly™ software (Comet Tech. Inc., Canada) were used to automatically identify resolvable (>5 voxels; >40 μm) occurrences of Mg-rich phosphate. A 2.5D U-Net convolutional neural network was trained on five manually segmented slices and successfully predicted >99% (Dice score = 0.997) of manually labeled voxels. This process was repeated three times to assess uncertainty. The average volume of Mg-rich phosphate is 1.3 ± 0.2 mm^3, and the total volume of the stone is 214.2 ± 2.1 mm^3 (whole-volume segmentation procedure and 1% relative uncertainty are based on methods from Ryan et al., 2026). The volumetric abundance of resolvable phosphate is 1.3% ± 0.2%.

El was performed at the University of Arizona Lunar and Planetary Laboratory. All EDS analyses were performed at 15 kV, 20 nA, 1 μm beam size. Wavelength-dispersive spectral (WDS) analyses were collected at 15 kV, 10 nA, 15 kV, 10 nA, 20 s peak counting time with a 2 μm beam size for normal matrix minerals and a 1 μm beam size for C-rich material. Well-characterized natural and synthetic materials were used as standards.

Visible and Near-Infrared (VNIR) Spectroscopy

VNIR spectra were measured at both the University of Winnipeg and Brown University. At the University of Winnipeg, sample OREX-800029-0 was poured into a black aluminum cup with a tapered 12.50 mm diameter, 3.25 mm deep well (Figure 1). The sample cup was gently tapped, and the edge of a clean glass slide was drawn across the sample to produce an approximately flat surface. Repeat measurements of the sample were made after mixing the sample with a stainless-steel needle (to expose different grains) and re-smoothing the surface. Reflectance spectra over the 350–2500 nm range were acquired with an Analytical Spectral Devices (Boulder, CO) LabSpec 4 Hi-Res spectrophotometer with an incidence (*i*) angle of 30° and emission (*e*) angle of 0° using a collimated, in-house 150 W quartz–tungsten–halogen light source operated at 70 W for sample illumination. All measurements were conducted in air (23.7–24.9°C, 6.8%–9.3% RH) over a few hours, and no brightening of the spectra was observed with time. Spectral resolution varies between 3 and 6 nm and spectral sampling is 1.4 nm. The data are internally resampled with a third-order polynomial to output data at 1 nm intervals. A total of 1000 spectra of sample, standard, and dark current were acquired and averaged to improve the signal to noise ratio (SNR). To further improve SNR, we collected multiple 1000 spectra sets and averaged them. Reflectance spectra were measured relative to a calibrated Fluorilon® disk and wavelength calibration was monitored with a

Ho_2O_3-doped Spectralon® standard (both made of polytetrafluoroethylene, PTFE). The ASD spectrometer has three detectors that collectively cover the full 350–2500 nm range as follows: 350–1000, 1000–1830, and 1830–2500 nm. There can be small reflectance offsets where detector changeovers occur (1000 and 1830 nm) and they are removed by multiplicatively scaling the shortest (350–1000 nm) and longest (1830–2500 nm) intervals to the middle interval (1000–1830 nm). Measuring non-diffuse and dark samples can lead to spectral artifacts, particularly in the 1000–1400 nm region that are recognizable and can be ignored. The spot size viewed by the spectrometer was as small as ~1.8 mm and as large as 4.0 mm, which allowed larger grains to nearly completely fill the field of view of the spectrometer. Both bulk powder and single grain dominated reflectance spectra were acquired.

VNIR spectra measured at Brown University were measured in bi-directional reflectance (BDR, 0.3–2.6 μm) for samples OREX-800029-0 and OREX-800073-0 using standard RELAB protocols [https://sites.brown.edu/relab/]. The sample particles were placed in a 14 or 9 mm diameter black (Teflon coated) dish (Figure 1). The measured spot size was ~8.8 or 7.2 mm diameter and the viewing geometry was $i = 30°$, $e = 0°$, phase angle (g) = 30° (all in the same plane). Data are calibrated against a Spectralon® target. The error on the as-measured spectrum corresponds to the standard deviation during the measurement of the sample. The as-measured reflectance was converted to normal albedo ($i = 0°$, $e = 0°$) by applying a scalar of 2.56, derived from the OSIRIS-REx Camera Suite (OCAMS) v-band (0.55 μm) phase and disk functions (Golish, Shultz, et al., 2021). Although there is presumably some wavelength dependence to the phase and disk functions—which characterize the angular distribution of scattered light and how brightness varies across a resolved body, respectively—these are unknown currently (OCAMS MapCam data indicate minor variations at visible wavelengths). Given these unknown characteristics, we have applied uncertainties of the same scale at all wavelengths, using bounding values of 2.5 and 2.6 for the lower and upper limits, respectively. For reference, MapCam yielded a normal albedo value of ~0.044 at 0.55 μm, but this value may be lower by ~10%–15% than true values. The samples were also measured in biconical reflectance using a Thermo Nexus 870 Fourier transform infrared (FTIR) spectrometer (0.9–100 μm) equipped with a diffuse reflectance attachment to obtain data at >2.55 μm. It is possible that some particles will have shifted slightly when moving from BDR to FTIR instruments. The FTIR measurement spot size was ~4 mm (the widest aperture). Spectra were acquired in air over several different wavelength ranges using different combinations of light sources and beamsplitters (e.g., CaF_2 and white light for NIR; KBr and Globar source for mid-IR) [https://sites.brown.edu/relab/]. FTIR spectra tend to be much darker than VNIR spectra because the diffuse gold standard is a highly anisotropic scatterer (i.e., reflection properties depend on angle of incidence as well as viewing angle). Therefore, the brightness of FTIR spectra should not be trusted and, although they are shown as measured in this work, is commonly scaled to the VNIR reflectance at ~2.5 μm.

Thermal Infrared (TIR) Spectroscopy

TIR spectra of polished sections were measured at Southwest Research Institute—Boulder using a Thermo Scientific Nicolet iN10 Fourier transform infrared microscope (μ-FTIR). This spectrometer is equipped with a liquid N_2-cooled, extended wavelength (MCT-B) detector for total coverage from 4000 to 400 cm^{-1} (2.5–25 μm). User-selectable parameters include spectral sampling, aperture size, and number of scans, which are recorded in the data files. These parameters are typically optimized to achieve high SNR without requiring excessively long analytical durations. The polished sections were measured in air with 2 cm^{-1} sampling and over 256 scans with a spot size of either 100 × 100 μm and map step size of 100 μm or 300 x 300 μm and 300 μm; the average of each map is shown. The single beam spectra are ratioed to a polished gold plate (measured at the same number of scans and sampling) to obtain reflectance. The uncertainty associated with cited band minima or peaks depends on the spectral resolution of the data at the time of acquisition. For data collected at 2 cm^{-1} sampling, the uncertainty in position is estimated to be on the order of one sample or ±2 cm^{-1}. The optics consist of a permanently aligned, 15×, 0.7 N.A. (half angle range 20°–43.5°) visible/IR objective and condenser. Given this relatively small angle, these reflectance spectra do not suffer from the band broadening effects near the Christiansen feature observed in biconical systems having large solid angles that include near-grazing angles of incidence and collection (Salisbury et al., 1991). As a result, we apply Kirchhoff's Law to invert these data (emissivity = 1 – reflectance) for direct comparison with emissivity data collected by OTES.

Polished samples present some spectral differences from loose particulates. The smooth surfaces of the sections enhance reflectance relative to particulates that scatter more of the incident light (e.g., Klima & Pieters, 2006). Crystallographic orientation effects may be visible in individual spectra where the spot size is small relative to a mineral grain; this effect is averaged out in the map-averaged spectrum as no petrographic fabric is present. Any spectra that include a substantial contribution from epoxy, for example, measured off the

sample or on its edge, were excluded from our analysis. Epoxy in nominally porous areas or cracks, etc., can contribute spectral features to the overall averages shown here. This signature was largely subtracted from the average spectra of OREX-800088-11 (hummocky stone) and OREX-800023-16 (mottled stone) using a measurement of pure epoxy from an area adjacent to the sample on the respective polished sections with small residual features excluded. Sections OREX-800055-1 and OREX-800088-11 had no coating applied; the mottled section (OREX-800023-16) was measured after C-coating. The effect of C-coating on these spectra is minimal and consists largely of the introduction of a weak spectral slope.

TIR spectra of mottled particles from OREX-800072-0 were measured at Brown University as described above.

OVIRS and OTES Data

We calculated the average OVIRS spectrum shown here using a subset (N = 416) of the data collected during OSIRIS-REx's third Equatorial Survey (Simon et al., 2021). This spectrum is indistinguishable from the average of all spectra collected during this phase. The OTES type 1 and type 2 spectra are from Hamilton et al. (2021).

RESULTS

Visible to Near-Infrared Spectral Characteristics

The visible albedo and VNIR slope of the aggregate Bennu sample (Table 1) deviate from the asteroid average values (Figures 1 and 2). The 0.55 μm normal albedo (i = 0°, e = 0°) of ~0.055 ± 0.001 (Figure 2a) is higher than values obtained remotely for average Bennu (0.044 ± 0.002, Golish, DellaGiustina, et al., 2021) and the darker boulders (0.034–0.049, DellaGiustina et al., 2020), but within the range of those for the brighter boulders (0.049–0.074, DellaGiustina et al., 2020) and Hokioi crater before (Jawin et al., 2023) and after (Lauretta et al., 2022) sampling. The reflectance (i = 30°, e = 0°) spectra have a red slope at 0.40–2.5 μm (Lauretta et al., 2024), consistent with another aggregate sample (Lauretta et al., 2024) but inconsistent with >99% of the asteroid, which has a mean blue slope (3σ) over this range (Barucci et al., 2020). The exception is ~0.5% of the OVIRS spectra analyzed by Barucci et al. (2020), which have a red slope from 1.0 to 2.5 μm (2σ). Spectra of the mottled fragments (Table 1, Figure 1b) exhibit a strong blue slope and considerably greater reflectance, where the visibly brighter materials are hydrous Mg-rich phosphate likely exposed on fracture surfaces. Isolated bright particles of this phosphate are evident but constitute << 1% of the aggregate sample.

On Bennu, weak (1%–2% depth) bands at wavelengths <2.5 μm were identified at ~0.55–0.60, 0.8, 1.0, 1.05, 1.4, 1.8, and 2.3 μm (Simon, Kaplan, Cloutis, et al., 2020). These features were difficult to detect without the removal of the "background" global spectrum; variations in particle size, space weathering,

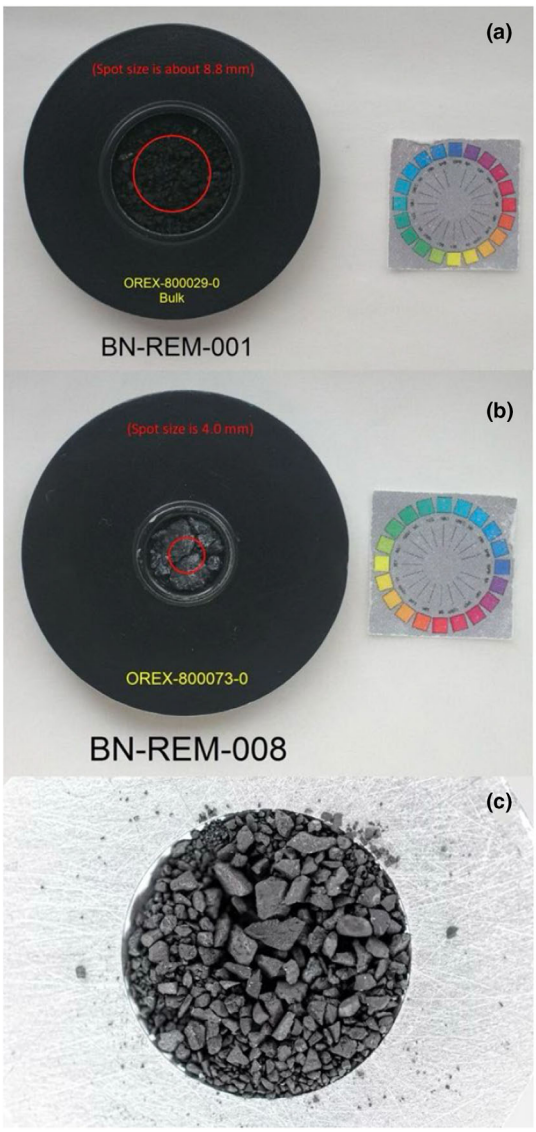

FIGURE 1. (a) Sample cup containing particles from OREX-800029-0 measured in bidirectional reflectance at Brown University. The well containing the sample is 14 mm in diameter. (b) Sample cup containing fragments from stone OREX-800073-0 measured in biconical reflectance at Brown University. The well containing the sample is 9 mm in diameter. (c) Sample cup containing particles from OREX-800029-0 aggregate sample as measured at University of Winnipeg. The well is 15 mm across.

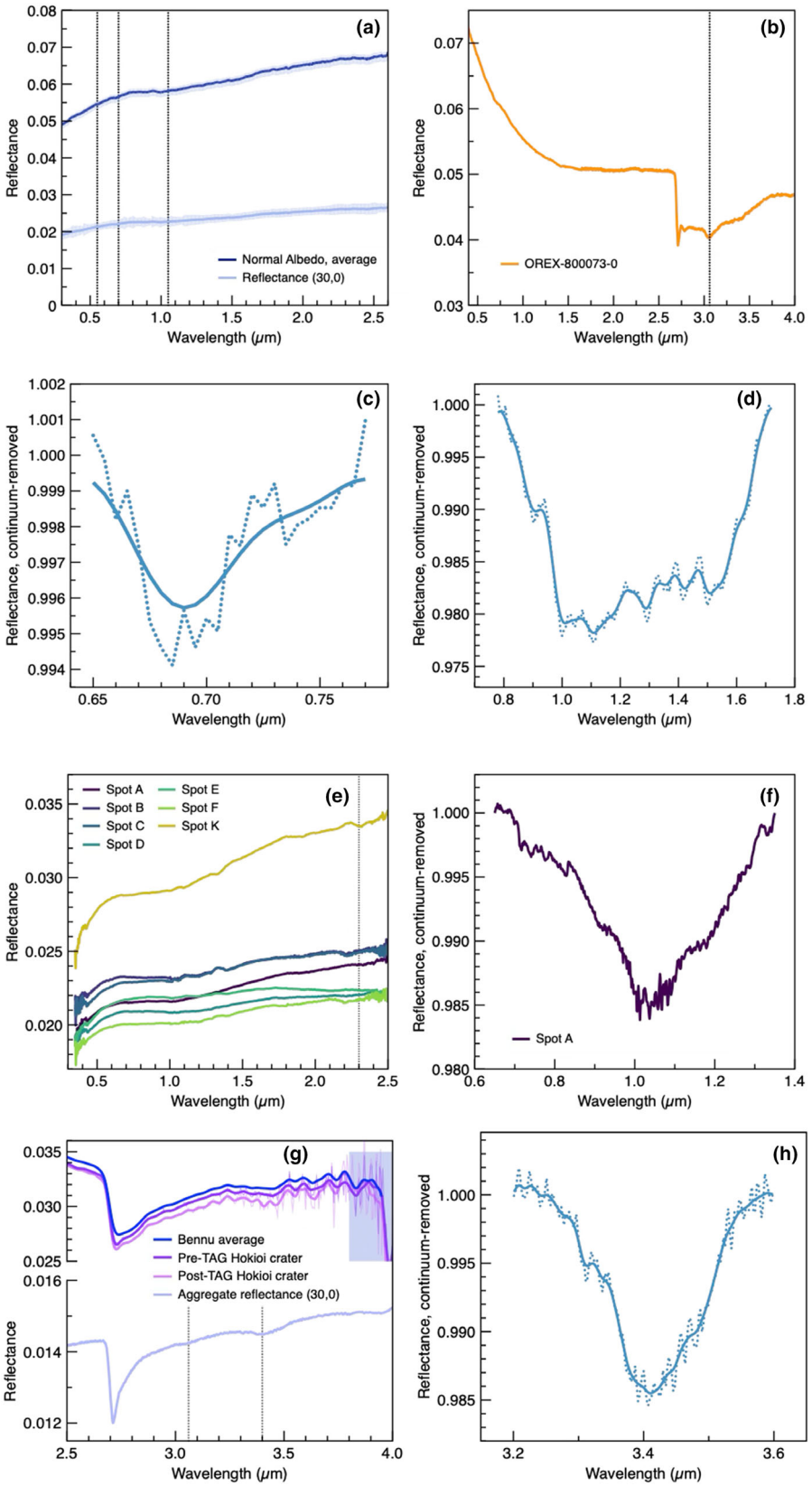
(a)
Reflectance
Wavelength (μm)
Normal Albedo, average
Reflectance (30,0)
(b)
Reflectance
Wavelength (μm)
OREX-800073-0
(c)
Reflectance, continuum-removed
Wavelength (μm)
(d)
Reflectance, continuum-removed
Wavelength (μm)
(e)
Reflectance
Wavelength (μm)
Spot A
Spot B
Spot C
Spot D
Spot E
Spot F
Spot K
(f)
Reflectance, continuum-removed
Wavelength (μm)
Spot A
(g)
Reflectance
Wavelength (μm)
Bennu average
Pre-TAG Hokioi crater
Post-TAG Hokioi crater
Aggregate reflectance (30,0)
(h)
Reflectance, continuum-removed
Wavelength (μm)

FIGURE 2. VNIR spectra of bulk aggregate sample OREX-800029-0 (all except b) and mottled particles (OREX-800073-0). Dotted lines highlight features of interest discussed in the text. (a) Average reflectance and conversion to normal reflectance (Methods). (b) Mottled particles exhibit a narrow minimum from OH^- at ~2.71 μm, broad H_2O band around 3 μm, and small N feature near 3.06 μm. (c) Continuum-removed spectrum of a possible hydration feature near 0.7 μm in the bulk aggregate. Solid line is a Gaussian smoothed (3σ) version here and elsewhere. (d) Continuum-removed bulk aggregate spectrum shows overlapping features at ~1–1.5 μm. (e) Spectra from distinct spots dominated by single particles. Some artifacts due to specular reflection are most apparent at 1–1.3 μm. (f) The unsmoothed, continuum-removed 1-μm region of Spot A (e). (g) Aggregate sample spectrum shown in (a) at wavelengths >2.5 μm (Methods), compared to OVIRS photometrically corrected global-average and local, before and after Touch-and-Go (TAG) sampling spectra of Bennu. Hokioi crater spectra with heavy lines represent a second-degree polynomial LOESS smoothing function applied to the original spectra (light lines). Shaded area indicates low signal-to-noise ratio. (h) Continuum-removed spectrum from (g) near 3.4 μm showing carbonate and/or organic features.

and other factors that can affect band centers and spectral slopes on Bennu are not duplicated by the measurement conditions of this aggregate, subsurface sample, which may explain why we do not detect these features in our sample spectra, except at ~0.7 and ~1.0–1.5 μm (Figure 1c,d). These features may be attributable, respectively, to Fe in phyllosilicates and combined features of serpentine, saponite, magnetite, and/or olivine. We found no strong absorptions at ~1.0 and 2.0 μm indicative of anhydrous phases in the aggregate sample, consistent with their minor abundances (Lauretta et al., 2024). Measurements focused on individual or small numbers of particles from the aggregate sample (Figure 2e) primarily show variations in overall reflectance and spectral slope that can be attributed to viewing conditions. The continuum-removed spectrum of "spot A" (Figure 2f) exhibits a broad, weak absorption in the ~1.0-μm region. A particle with dark and light areas, identified as "spot K", was the brightest and reddest seen in these data. It exhibits an absorption band at 2.32 μm (Figure 2e) that is most consistent with dolomite (Gaffey, 1986).

Above 2.5 μm, a minimum attributed to hydration (Figure 2g) occurs at a shorter wavelength (2.71 ± 0.0015 μm) in the aggregate sample compared with average Bennu (2.74 ± 0.01 μm, Hamilton et al., 2019) and Hokioi crater (2.72 μm, Deshapriya et al., 2021). Its position is characteristic of Mg—OH bonds in Mg-rich serpentine and saponite. The band is also considerably narrower than average Bennu and Hokioi crater (Hamilton et al., 2019; Praet et al., 2021), and there are no overtones of the fundamental H_2O bending mode at 3.1 μm. These data suggest that the aggregate sample has less total adsorbed and/or structural H_2O relative to the average optical (uppermost) surface of Bennu and is instead dominated by hydroxyl (Lauretta et al., 2024). A considerably broader H_2O feature is observed around 3 μm in the mottled fragments (Figures 1b and 2b), arising from highly hydrated Mg—rich phosphate.

A feature near ~3.06 μm—relatively weak in the aggregate sample (Figure 2g) but stronger in the mottled fragments (Figure 2b)—is consistent with N-bearing components. The N may occur in ammoniated organic compounds (Glavin et al., 2025), a recently discovered N-rich polymeric organic material (Sandford et al., 2025), clay minerals or an ammonium-bearing phosphate like struvite, $MgNH_4PO_4{\cdot}6H_2O$ (Pilorget et al., 2024). The aggregate sample shows weak bands at 3.4 and 3.8–4.0 μm (Figure 2g,h) indicative of C-bearing compounds. These features are primarily attributable to carbonate, particularly calcite and dolomite (Lauretta et al., 2024). Aliphatic C-H stretching modes also can contribute near 3.4 μm (Kaplan et al., 2020).

Thermal Infrared Spectral Characteristics

Spectra from sections of the angular, hummocky, and mottled stones (Table 1) are dominated by silicate features (Figures 3 and 4a,b). The Christiansen feature occurs at ~1115 cm^{-1} in the angular stone, ~1108 cm^{-1} in the hummocky stone, and ~1070 cm^{-1} in the mottled stone. The first two values are consistent with spacecraft observations of Bennu (Hamilton et al., 2019, 2021), whereas the feature position in the mottled stone is not. All three stones exhibit a minimum near 1000 cm^{-1}, characteristic of silicate stretching fundamental bands. The angular and hummocky samples have relatively narrow, asymmetric V-shape absorptions with convex-up or limited curvature, respectively, characteristic of mixed serpentine and saponite phyllosilicates with variable degrees of order like those in CI chondrites (Hamilton et al., 2021). The mottled sample exhibits a broader, more rounded absorption with opposing asymmetry, slight concave curvature, and a minimum shifted rightward to 925 cm^{-1}. A phyllosilicate Mg—OH deformation band occurs at ~700–530 cm^{-1} and a peak at 528 cm^{-1} in all three spectra is characteristic of poorly crystalline serpentine and saponite-rich phyllosilicates. Features below 528 cm^{-1} can arise from silicates, carbonates, and oxides; all samples exhibit virtually identical minima near 440 cm^{-1} consistent with phyllosilicates and suggesting that phyllosilicate composition does not control the Christiansen feature position and spectral broadening in

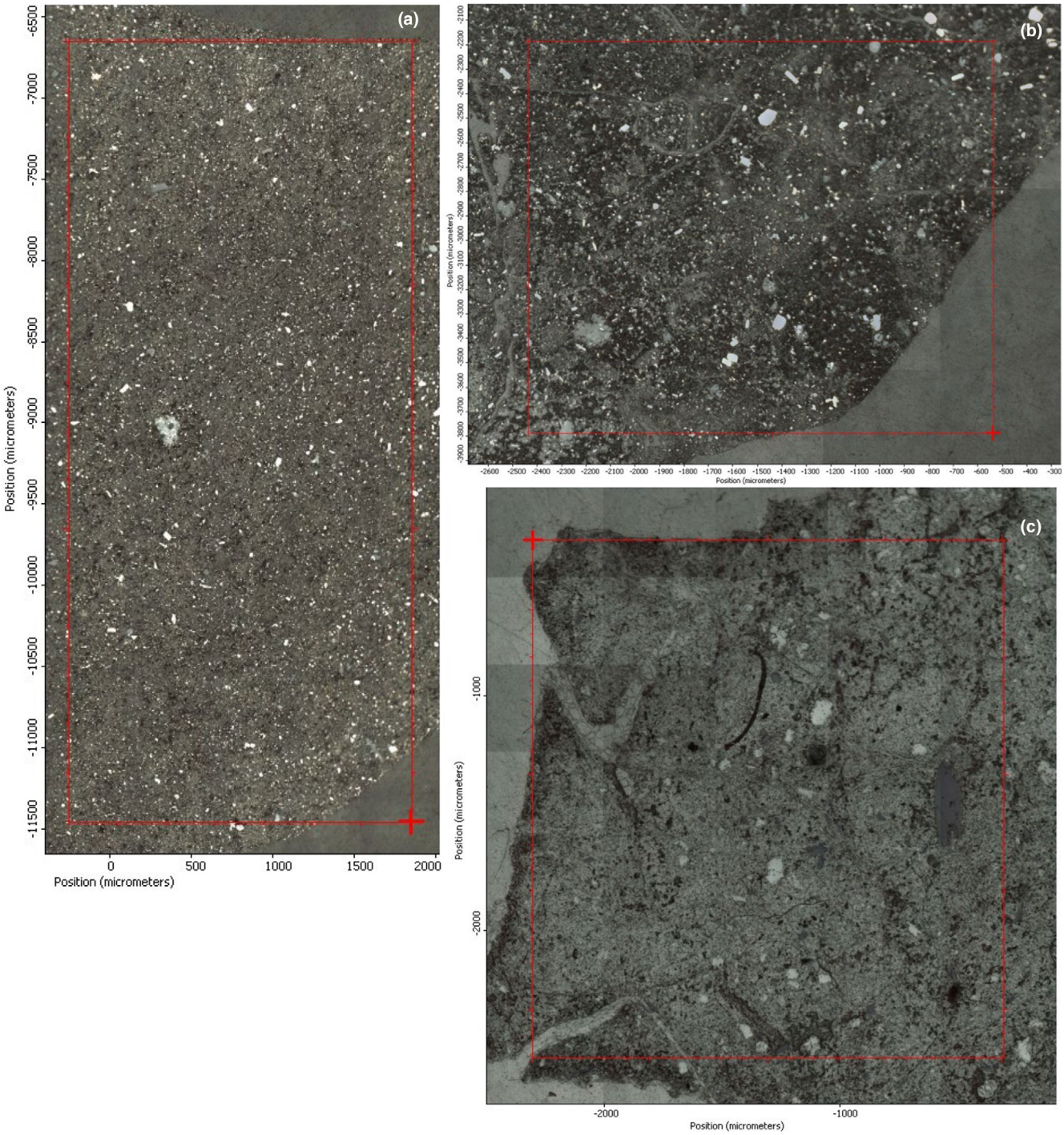

FIGURE 3. Reflected light images of polished sections showing areas from which averaged spectra were measured (red boxes and points). (a) OREX-800055-16 (angular), (b) OREX-800088-11 (hummocky), (c) OREX-800023-16 (mottled).

the mottled sample. No features of anhydrous silicates are evident.

Spectral features of carbonates, Mg-rich phosphate, and magnetite are present in the samples, along with aldehydes, a functional group associated with organic material (Figure 4a,b) (Matrajt et al., 2005). An asymmetric peak at 1430 cm^{-1} is consistent with both small crystallite carbonate (Hamilton et al., 2020) and Mg-rich phosphate (Figure 4a,b). Other carbonate features are present at 875, and 727 cm^{-1} and indicate a dolomite composition (Lane & Christensen, 1997). Due to its low areal abundance, Mg-rich phosphate does not

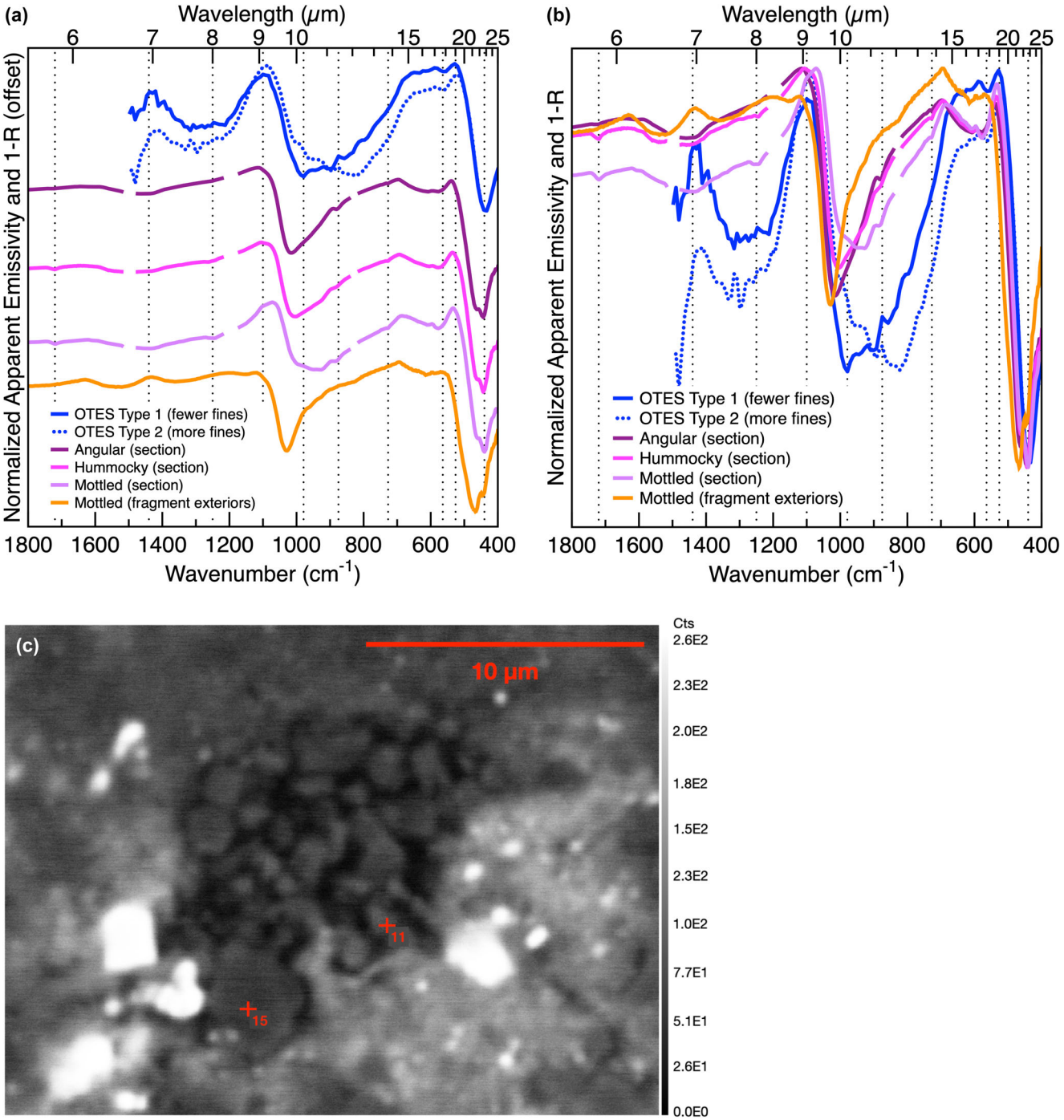

FIGURE 4. (a) OTES average spectra of Bennu regolith spectral endmembers, termed type 1 (fewer fines) and type 2 (more fines) (Hamilton et al., 2021); polished sections OREX-800055-1 (angular), OREX-800088-11 (hummocky), and OREX-800023-16 (mottled); and the exteriors of mottled particle fragments from OREX-800073-0. Laboratory sample spectra are shown offset from the OTES spectra. (b) The same spectra as in (a) without offset. Dotted vertical lines enable comparisons between spectra. On the y-axis, $1 - R$ is emissivity derived from reflectance (Methods). OTES data are shown at native 8.66 cm^{-1} spectral sampling, smoothed with a Gaussian filter of 1.0. (c) Backscattered electron image of a portion of OREX-800023-16 showing location of matrix material associated with broadened spectral feature and WDS analysis (point 15, Table 2).

contribute visibly to the TIR spectra of polished sections, but the spectrum of the mottled fragment surfaces exhibits Mg-rich phosphate minima at ~1525 and 1360 cm^{-1} and a peak near 1430 cm^{-1}. The larger, fundamental PO_4 absorptions (Lauretta et al., 2024) near 1070 and 925 cm^{-1} are not evident and there is a shift in the position of the lowest wave number feature relative to phyllosilicate. Magnetite produces a weak feature at ~555 cm^{-1}. C═O bonds in carbonyls (aldehydes) are evidenced by a feature at 1720 cm^{-1} in the hummocky and mottled stones.

We propose three potential explanations for the distinctive spectral character of the mottled stone section. First, there may be variation in the serpentine/saponite ratio or phyllosilicate composition. Sample analyses to date do not provide insight into these possibilities for mottled materials, but increased Fe has been observed in coarser grained phyllosilicates in a hummocky particle (Zega et al., 2025). Second, there may be differences in phyllosilicate nanoscale to microscale structure. Although not directly relatable to the scale of the spectral measurements, transmission electron microscopy of Bennu samples revealed fine- and coarse-grained sheet silicates at the scale of hundreds of nanometers and both poorly crystalline to amorphous and long-range ordered components (Zega et al., 2025). Third, a locally greater concentration of a non-silicate component, such as organic material, which is abundant in Bennu samples (Barnes et al., 2025; Lauretta et al., 2024), may influence the spectral shape.

The hypothesis of an enhanced concentration of organic material in the mottled stone section is supported by our EDS and WDS analyses of the section. These data indicate a greater abundance of organic C in this polished section that corresponds to a particularly broad spectral feature in some of the individual μ-FTIR map spectra. Localized areas with the unusual spectral feature were observed in backscattered electron (BSE) images (e.g., Figure 4c) to contain variable amounts of a dark (low-Z) phase intimately intermixed with the Bennu matrix. EDS spectra of several patches of this dark material (not shown) indicate that they all contain very high amounts of C and O, along with much lower to non-existent amounts of Si, Mg Ca, S, and Fe, which is consistent with these being variable mixtures of a C-rich phase and the phyllosilicate matrix. To further check this, WDS analyses were performed on the locations of the dark material that appeared to be the best separated from the surrounding matrix based on EDS spectra and BSE imaging. We observed that the WDS analyses were consistent with the EDS results, but with very low analytical totals (Table 2). For the best separated occurrence of the dark phase (Figure 4c, point 15), the WDS total was 1.17 wt%%, consisting of very minor measured Fe, Mg, and Si and O determined by stoichiometry. Cl was not detected, which indicates that the material is probably not the mounting epoxy, which is also supported by TIR spectra that lack epoxy features. As EDS indicated that no unmeasured elements other than C and O were present in these areas, in the absence of obvious beam damage, the low WDS totals suggest that the dark phase is probably mainly C, although some O may also be present. Thus, we interpret the dark phase areas in this sample, which correspond with the shifted TIR minimum at ~925 cm^{-1}, as a (probably organic) C phase, intermixed with matrix material. This material has also been examined by scanning electron microscopy (SEM) and NanoSIMS and shown to be primarily composed of C nanoglobule-like particles with non-anomalous C and N isotopic compositions (P. Haenecoeur, personal communication). These appear to be intimately mixed with O-rich materials that are most likely phyllosilicates and Fe framboids.

TABLE 2. WDS element and oxide abundances of dark phase associated with broadened band in TIR spectra of mottled sample section OREX-800023-16.

Element	wt%	Oxide	wt%
Na	0.00	Na_2O	0.01
Si	0.14	SiO_2	0.30
Mg	0.16	MgO	0.26
Al	0.01	Al_2O_3	0.03
K	0.01	K_2O	0.01
Ti	0.00	TiO_2	0.00
Ca	0.01	CaO	0.01
Fe	0.34	FeO	0.44
Mn	0.00	MnO	0.00
Cr	0.01	Cr_2O_3	0.01
P	0.01	P_2O_5	0.02
S	0.01	SO_3	0.04
Ni	0.03	NiO	0.03
Cl	0.01	Cl	0.01
O	0.43	FeO	0.01
Total	1.17	Total	1.17

DISCUSSION

Connecting Bennu Samples to OSIRIS-REx Remote Sensing

The sample spectra presented here diverge considerably from the average global spectral characteristics of asteroid Bennu. This discrepancy is probably because the samples, which come from depths of 0 to 0.5 m (Lauretta et al., 2022), are not fully representative of the uppermost surface that is observable remotely, and much smaller areas are measured in the

laboratory than remotely. The difference in the VNIR spectral slope between the asteroid and the samples may be explained by several factors. Variations in the degree of space weathering could alter surface reflectance through the accumulation of nanophase Fe-Ni-S particles (e.g., Hapke, 2001; Pieters et al., 2000). Different proportions of organics, high-albedo phases, or opaque minerals in the small areal field of view of laboratory spectrometers can contribute to differing absorption features, reddening, or change the overall brightness and spectral contrast relative to OVIRS and OTES spectra. Differences in bulk composition, particle size distributions, and surface texture further influence light scattering and absorption. Finally, the conditions under which spectra are collected (remotely and in the laboratory), such as viewing geometry, illumination, and detector sensitivity, can also modify the observed slope. These influences make it difficult to uniquely determine the origin of the discrepancies. Here, we consider space weathering, composition, and particle size effects.

The Hokioi crater sampling site was selected primarily because it was deemed safe and contained fine regolith ingestible by the OSIRIS-REx sampler. It is spectrally less blue than global average Bennu, and it became even less so after sampling (Figure 2d and Lauretta et al., 2022), consistent with models of space weathering (Clark et al., 2023; Keller et al., 2025) and the reduction in average particle size (Barucci et al., 2020). Although there is physical evidence for some space weathering in Bennu contact pad samples (Keller et al., 2025), the narrow and shorter wavelength OH— feature (2.71 μm) in the aggregate sample we analyzed also is consistent with that of the relatively fresh surface in Hokioi crater (2.72 μm) and in contrast to that of the older, global average surface (~2.74 μm). Such band shifts and peak broadening are observed in experimental space weathering of the Alais (CI1) and Tagish Lake (C2-ungrouped) meteorites (Lantz et al., 2017). Water can be produced by space weathering (e.g., Bradley et al., 2014), but the width of the 3 μm band is virtually invariant on Bennu, including at Hokioi crater before and after sampling, suggesting that older and younger surfaces have similar hydration states (Barucci et al., 2020; Praet et al., 2022).

The identification of Mg-rich phosphate (McCoy et al., 2025) offers an alternative interpretation (Lauretta et al., 2024) of the composition of relatively high-albedo, linear, and mottled surface features observed on some Bennu boulders, which were initially interpreted as carbonate veins based on spacecraft spectra (Kaplan et al., 2020). However, if these are instead Mg-rich phosphates, the 3 μm region, might be expected to exhibit a wider H_2O band than the average surface, but it does not (Figure 5). The widespread presence of carbonate in the returned sample (Connolly Jr et al., 2025; McCoy et al., 2025) further supports the interpretation of bright material on Bennu as carbonate. Nonetheless, phosphate may contribute to the global spectral properties.

X-ray computed tomography indicates the total abundance of hydrous Mg-rich phosphate in one mottled stone is 0.5%–1.5% by volume, which, if representative, implies a low likelihood of spectral detection, assuming equivalence with area. The areal fraction of bright material on boulders has not been determined, but a visual estimate from the returned sample, that is, figure 5 in Lauretta et al. (2024), suggests on the order of 2%–3.5% by area. Reflectivity is a function of wavelength and is known to vary non-linearly with viewing geometry, illumination, and surface slope; this non-linearity is particularly evident in cases where scattering (high albedo) or absorption (low albedo) dominates. If some of the rocks on Bennu have concentrations of relatively bright, Mg-rich phosphate on exposed (fractured) vein surfaces, remote measurements could be influenced disproportionately, imparting non-linear effects on the asteroid's visible spectral slope (blueness), contributing H_2O at 3 μm, and increasing the global albedo relative to the darker, redder aggregate material in Hokioi crater (Deshapriya et al., 2021; Lauretta et al., 2022). A quantitative spectral model and a physical process for concentrating mottled material at the surface have yet to be explored and reconciled with evidence of space weathering, but if Mg-rich phosphates contribute substantially to Bennu's blue spectral slope, then the B-type asteroids may exhibit similar exposures. This raises the question of whether B-type asteroids possess inherently higher abundances of hydrous phosphates due to their unique bulk compositions, or if secondary processing has resulted in enhanced surface exposures of this material.

In situ spectral data are sensitive to the upper tens to hundreds of microns of Bennu's surface, and those from OTES exhibit band broadening that was ascribed to very minor, but variable, deposits of fine particulates producing weak volume scattering (Hamilton et al., 2021). Because our polished-section spectra do not exhibit volume scattering and resemble CI(−like) materials, we conclude that the broadened OTES spectral shapes are almost certainly attributable to thin and/or patchy deposits of fine particulates, an insight that confirms thermophysical models of the surface (Rozitis et al., 2020) and constrains the nature of particle size effects in OVIRS data. It also demonstrates that spectra of solid meteorites measured in ambient conditions are important TIR spectral analogs for small, dark, fast-rotating asteroids. Traditionally, the spectroscopy community has generally assumed that powdered samples (e.g., ≤˜65 μm) are the best analogs to asteroid surfaces in the VNIR and TIR (relative to coarse

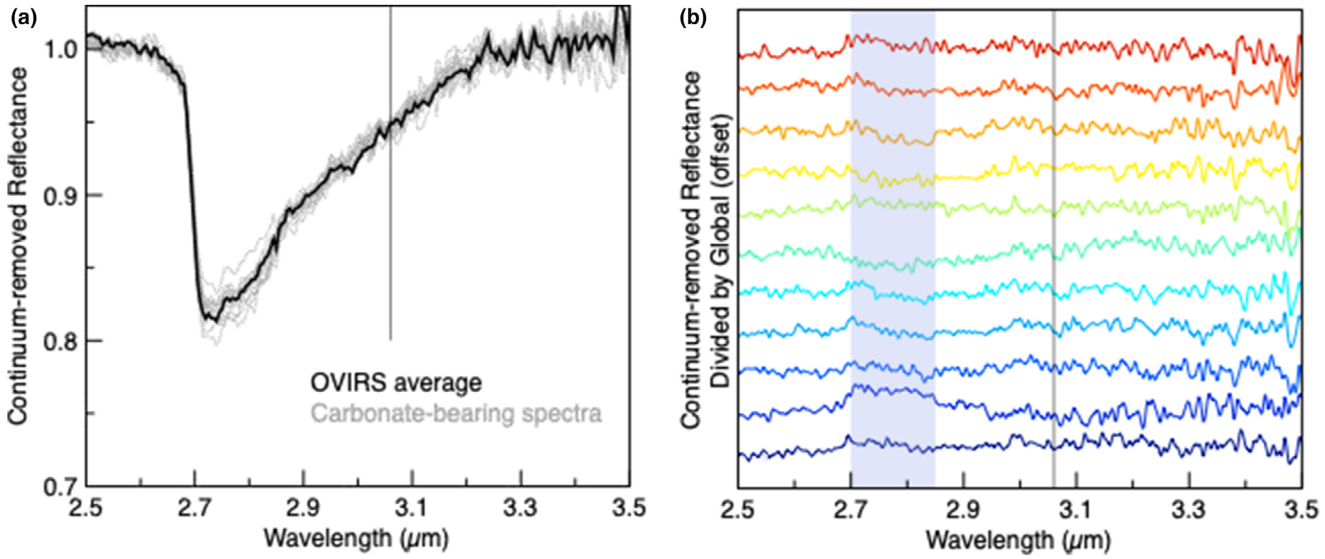

FIGURE 5. (a) Twelve reconnaissance-phase, continuum-removed (2.6–3.3 μm) OVIRS spectra of proposed carbonate vein-bearing materials (Kaplan et al., 2020) compared to average Bennu. Variability in the 2.74 μm band depth may result from differences in viewing geometry or other factors independent of abundance. (b) Spectra of proposed carbonate-bearing materials from (a), divided by the OVIRS average in (a). Blue-shaded area indicates region of band depth variations and an OVIRS filter function near 2.75 μm. No significant deviations are apparent between ~2.85 and 3.3 μm that suggest a discernible increase in the width of the 3 μm band or the appearance of a feature at 3.06 μm indicative of N-bearing compounds.

particulate or solid samples) because they (1) exhibit spectral effects of the greater scattering that occurs in powders and (2) show effects of vertical thermal gradients that might be introduced in fine particulates on airless bodies as theorized for the Moon by, for example, Logan and Hunt (1970) and Henderson and Jakosky (1997). However, the relatively higher thermal inertias commonly associated with small, fast-rotating asteroids (Delbó et al., 2007) suggest that their mean particle sizes are not equivalent to powders (and as we have seen at Bennu, considerably larger than predicted). Additionally, carbonaceous materials have exceedingly low albedo as compared to the Moon, which inhibits the absorption of visible energy at depth, in turn preventing the production of thermal gradients. Therefore, solid sample spectra of carbonaceous materials are important analogs to include in spectral libraries used for the TIR spectral analysis of small, carbonaceous asteroids.

The phyllosilicate Mg—OH feature at 700–532 cm^{-1} was weak in OTES spectra but is readily observed in the three polished sections. Its absence in OTES data was attributed to material heating (Hanna et al., 2023), space weathering (Hanna et al., 2023), and/or a physical effect like scattering in fine particulates or side-welling radiance (Hamilton et al., 2021). We see no spectral evidence for post-aqueous alteration heating of the sample. Spectra of space-weathered CI and CI-like meteorites have not been shown in this spectral region (Lantz et al., 2017), but particle size and side-welling radiance effects remain plausible at Bennu. OTES spectra exhibit a peak at ~1420 cm^{-1} that was attributed to either fine particulate carbonate or sulfide in solid or coarse particulate form. This peak is not apparent in our polished section spectra, indicating that sulfide (present in all three stones) is not producing it. This position is close to the small crystallite carbonate minimum seen in the average spectra of the sections. The peak in Bennu data could be carbonate appearing in emission because the strong carbonate absorption occurs in a region where fine particulate silicates are only weakly absorbing (Bandfield et al., 2003). A feature in virtually all OTES spectra at ~874 ± 9 cm^{-1}, suggested to represent carbonate (Hamilton et al., 2022), is evident in our sample spectra where carbonate is present and suggests that carbonate may be dispersed widely in small amounts across the surface of Bennu. Mg-rich phosphate on mottled stones also exhibits a peak near ~1420 cm^{-1} (Figure 4) and may contribute to this OTES spectral feature. The absence of strong Mg phosphate fundamental bands in the mottled stone fragments suggests that such features may be difficult to detect at Bennu.

Comparison to Meteorites and Ryugu

In the classification scheme of Van Schmus and Wood (1967), petrologic type 3 carbonaceous chondrites are effectively unaltered or only minimally altered, type 2 are increasingly aqueously altered, and type 1 are the

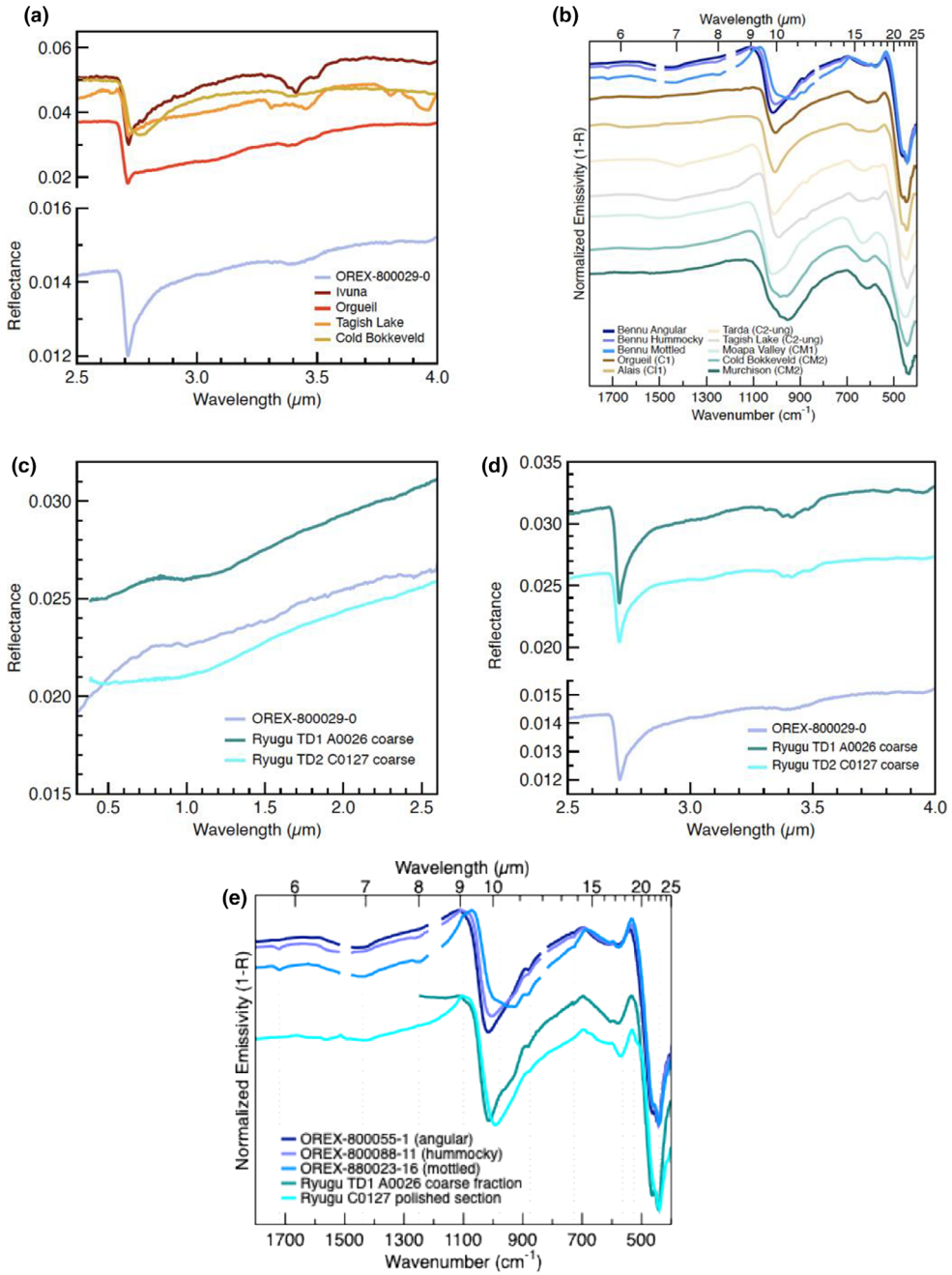

FIGURE 6. Comparisons of Bennu sample spectra with carbonaceous chondrites and Ryugu samples. (a) A Bennu aggregate sample compared to analog CI and C2-ungrouped meteorites. The meteorites were measured under vacuum (Nakamura et al., 2022; Takir et al., 2013). (b) Bennu polished section spectra from Figure 4 compared to polished section spectra of analog meteorites (Hamilton et al., 2021). The peak at ~528 cm^{-1} in the sample spectra constrains the best meteorite analogs and is uniquely diagnostic of serpentine + saponite. (c, d) Bennu aggregate spectrum from Figure 2 compared to coarse Ryugu samples from 0.4–2.6 and 2.5–4.5 μm (Nakamura et al., 2022). (e) Bennu polished section spectra from (b) compared to coarse Ryugu sample A0026 (Nakamura et al., 2022) and polished section of particle C0127 (Goodrich et al., 2023).

most aqueously altered. At all wavelengths shown here, Bennu sample spectra look most like those of the type 1 CI chondrites and two strongly altered type 2 C chondrites (ungrouped), Tagish Lake and Tarda, as opposed to less altered CM2 chondrites (Hamilton et al., 2021) (Figure 6). This resemblance is consistent with similar bulk compositions dominated by poorly ordered serpentine and saponite phyllosilicates (Bates et al., 2024;

Nakamura et al., 2022; Zega et al., 2025). Nevertheless, there are no good analogs to the average TIR polished section spectrum of the mottled stone's matrix among the 73 representative CI, CM, and C chondrite (polished section) spectra we considered. This result strongly suggests that portions of the matrix of the Mg-rich phosphate-bearing mottled stones have no spectral analog in our meteorite collections.

Ryugu is a carbonaceous asteroid like Bennu, but it is not a B type; its global spectrum is red (Nakamura et al., 2022). Spectra of Ryugu (Goodrich et al., 2023; Nakamura et al., 2022) samples share these meteorite analogs, contain hydrous phosphate, and bear N in ammoniated components (Glavin et al., 2025; Pilorget et al., 2024). These commonalities suggest that both asteroids (or their components) originated in a common reservoir in the outer solar system, where ammonia was stable, and experienced similar evolutionary histories (Glavin et al., 2025). The VNIR spectra of aggregate Bennu and Ryugu samples (and the Ryugu surface) are similar in terms of overall reflectance, spectral slope, and 3 μm band shape (Figure 6). However, the TIR phyllosilicate Si-O stretching absorption positions are not identical in Bennu and Ryugu samples analyzed to date (Figure 4).

Differences between the Bennu and Ryugu spectra in the TIR may be attributable to one or more characteristics. First, slightly different cation compositions between Bennu and Ryugu serpentines (or saponites or both) could result in relative band minimum shifts (Calvin & King, 1997). Second, different proportions of serpentine and saponite may alter the combined band shape and minimum position. Third, different proportions of fine- and coarse-grained phyllosilicates differences (differing in crystallite size but not composition) can change band minima positions and shapes (Hamilton et al., 2020). Finally, differences in space-weathering exposure (Keller et al., 2025) produce variable amounts of band shift due to effects such as preferential loss of Mg relative to Fe, amorphization, and deposition of nanophase metallic iron (e.g., Lantz et al., 2017). No analog for the TIR spectrum of the mottled stone matrix measured here has been identified yet in the Ryugu sample, indicating further differences between their compositions or the localized concentrations of components. Depending on the proportion of mottled material exposed at Bennu's surface, these differences could be substantial at the asteroidal scale.

There are unresolved differences between the asteroids' VNIR slopes and 3 μm band shapes, which may be attributable to space weathering (Clark et al., 2023; Deshapriya et al., 2021; Keller et al., 2025) and/or a greater concentration of a hydrated phase—possibly Mg-rich phosphate—at Bennu's surface. Due to the small number of particles extracted from the OSIRIS-REx contact pads, spectra of the surfaces of space-weathered materials from Bennu are not yet available, but we can consider implications from other data. Similar shortward shifts at ~2.7 μm were observed by Hayabusa2 at Ryugu at the site of the Small Carry-on Impactor experiment (Kitazato et al., 2019) and may be an effect of space weathering (Hiroi et al., 2023). Ryugu and Bennu samples exhibit space-weathering features including melts, solar wind–damaged rims, and microcraters (Keller et al., 2025; Noguchi et al., 2022), indicating comparable space weathering occurs on both asteroids albeit with differences in surface exposure time. Although Bennu exhibits a globally blue spectral slope and Ryugu a red one, spectra of both asteroids' youngest surfaces and samples are flat to red-sloped, consistent with relatively less space weathering and observations that their sampled subsurface materials share a common composition (DellaGiustina et al., 2020; Yumoto et al., 2024). The broader 3 μm feature on Bennu relative to Ryugu (Kitazato et al., 2019) may indicate a greater proportion of hydrous phosphate exposed at the surface of Bennu contributes to the blue slope. A plausible interpretation is that both space weathering and hydrated Mg-rich phosphate contribute to Bennu's global VNIR spectrum, which may be tested by quantitative models and/or laboratory measurements. Such analyses may be able to determine whether there is a threshold abundance or physical configuration at which the spectral effects of hydrous phosphate transition from linear to non-linear. Ultimately, any quantitative model for Bennu's VNIR spectrum must address its blue slope, the lower reflectance of the aggregate sample and younger surfaces in general, and the invariant shape of the 3 μm hydration band. It must also be consistent with the overall mineralogy, physical space-weathering features, spectral feature and rock type variations as a function of geology, and the spectral character and particle size implications of the scattering behavior observed in OTES data.

CONCLUSIONS

Analysis of Bennu samples demonstrates that spacecraft can obtain highly accurate compositional information about dark, carbonaceous asteroids, including the detection of some low-abundance (few percent) phases such as magnetite and carbonate. Ongoing re-evaluation, across all wavelengths, of the spacecraft data and modeling of the sample spectra will establish whether spectral features of Mg-rich phosphate are detectable with hindsight and provide implications for future spacecraft observations. OSIRIS-REx is the first mission to a small body demonstrating the use of TIR spectroscopy for characterizing asteroid compositional and physical

properties. OTES data revealed fundamental absorptions of magnetite (Hamilton et al., 2019), placed quantitative limits on the abundance of phyllosilicates and anhydrous silicates (Hamilton et al., 2021), and narrowed constraints on the matrix phyllosilicate composition (Hamilton et al., 2021). Physical properties such as particle size distribution can greatly affect asteroids' VNIR spectral properties, and the limited volume scattering evidenced in OTES spectra constrains the particle sizes and approximate thicknesses of dust on Bennu's surface (Hamilton et al., 2021). These data provide a benchmark for estimates of particle size differences among similar carbonaceous asteroids, which may not be discernible from thermal inertia and underscores the importance of collecting analog spectra from solid samples in addition to powders. Information at TIR wavelengths can substantially augment primitive asteroid classifications (DeMeo et al., 2009), our understanding of their likely compositions and dominant particle sizes (Hamilton et al., 2021), and the compositional diversity among primitive bodies having different visible spectra and variable space weathering (Yumoto et al., 2024). Future missions to primitive asteroids (and other small bodies) should consider that OSIRIS-REx achieved such accuracy in determining Bennu's composition by having visible through thermal infrared data, that is, leveraging a wide wavelength range. Neither data set alone would have permitted as complete a characterization of Bennu's composition prior to sample return.

The similarities of Bennu and Ryugu to the rare CI carbonaceous chondrites is further evidence that our understanding of these meteorites' characteristics and prevalence among the asteroid population is poor because they are not well represented among our collections and can be rapidly altered by exposure to the terrestrial environment. The asteroidal signatures may express compositional differences from meteorites and/or obscuration by space weathering. The spectral similarity of phyllosilicate-rich Bennu and Ryugu samples to the ungrouped type 2 meteorites Tagish Lake and Tarda may offer greater insight into possible links between Ryugu and Bennu's parent bodies and the D-type asteroids, soon to be observed by the Lucy mission (Levison et al., 2021), that have been proposed as a source for those meteorites (Schrader et al., 2024).

B-type asteroids are disproportionately represented among bodies with past or inferred comet-like activity, such as (3200) Phaethon (e.g., Licandro et al., 2007). Their spectral properties may provide insight into volatile content, alteration history, and mineralogies not captured in current meteorite collections. However, their blue spectral slopes have been challenging to explain, making broader inferences difficult. Spectra of Bennu aggregate samples deviate substantially from signatures of the asteroid's surface in the VNIR and therefore are not spectrally representative at telescope-relevant scales, requiring us to continue to speculate on the origin(s) of blue slopes. Experimental and modeling efforts (Loeffler & Prince, 2022; Trang et al., 2021) have shown that opaque phases, such as magnetite and graphite, and space weathering contribute to spectral bluing. Magnetite has been identified at Bennu and possibly on other B types (Yang & Jewitt, 2010). Blue-sloped, Mg-rich phosphates observed in the Bennu samples offer a possible additional factor influencing spectral slopes on hydrated carbonaceous bodies, particularly for populations with evidence for water (H_2O) or where bluing cannot be explained solely by space weathering or viewing geometry.

Acknowledgments—This material is based on work supported by NASA under Contract NNM10AA11C issued through the New Frontiers Program. EAC acknowledges support from the Canadian Space Agency (grant 22EXPOSIWI). N. B. and K. A. S. acknowledge support from UK Science and Technology Facilities Council (grant ST/W000938/1). The authors thank T. Nakamura for sharing the digital data from their cited works, and we appreciate the editorial assistance of C. W. V. Wolner. We acknowledge the entire OSIRIS-REx team for enabling the return and analysis of Bennu samples and the OSIRIS-REx Curation team at JSC for their extraordinary care and preparation of Bennu materials.

Conflict of Interest Statement—None of the authors have a conflict of interest to disclose.

Data Availability Statement—The data that support the findings of this study are openly available in Astromat at https://www.astromat.org.

Editorial Handling—Dr. A. J. Timothy Jull

REFERENCES

Bandfield, J. L., Glotch, T. D., and Christensen, P. R. 2003. Spectroscopic Identification of Carbonate Minerals in the Martian Dust. *Science* 301: 1084–87.

Barnes, J. J., Nguyen, A. N., Abernethy, F. A. J., Bajo, K., Bekaert, D. V., Bloch, E., Brennecka, G. A., et al. 2025. The Variety and Origin of Materials Accreted by Bennu's Parent Asteroid. *Nature Astronomy* 9: 1785–1802. https://doi.org/10.1038/s41550-025-02631-6.

Barucci, M. A., Hasselmann, P. H., Praet, A., Fulchignoni, M., Deshapriya, J. D. P., Fornasier, S., Merlin, F., et al. 2020. Osiris-rex Spectral Analysis of (101955) Bennu by Multivariate Statistics. *Astronomy & Astrophysics* 637: L4. https://doi.org/10.1051/0004-6361/202038144.

Bates, H. C., Aspin, R., Fu, C. Y., Harrison, C. S., Feaver, E., Branagan-Harris, E., King, A. J., Bryson, J. F., Sridhar, S., and Nichols, C. I. 2024. Extent of Alteration,

Paleomagnetic History, and Infrared Spectral Properties of the Tarda Ungrouped Carbonaceous Chondrite. *Meteoritics & Planetary Science* 59: 2411–31. https://doi.org/10.1111/maps.14224.

Bradley, J. P., Ishii, H. A., Gillis-Davis, J. J., Ciston, J., Nielsen, M. H., Bechtel, H. A., and Martin, M. C. 2014. Detection of Solar Wind-Produced Water in Irradiated Rims on Silicate Minerals. *Proceedings of the National Academy of Sciences of the United States of America* 111: 1732–35.

Calvin, W. M., and King, T. V. V. 1997. Spectral Characteristics of Iron-Bearing Phyllosilicates: Comparison to Orgueil (Ci1), Murchison and Murray (Cm2). *Meteoritics & Planetary Science* 32: 693–701.

Christensen, P. R., Hamilton, V. E., Mehall, G. L., Pelham, D., O'Donnell, W., Anwar, S., Bowles, H., et al. 2018. The Osiris-rex Thermal Emission Spectrometer (Otes) Instrument. *Space Science Reviews* 214: 87. https://doi.org/10.1007/s11214-018-0513-6.

Clark, B. E., Binzel, R. P., Howell, E. S., Cloutis, E. A., Ockert-Bell, M., Christensen, P., Barucci, M. A., et al. 2011. Asteroid (101955) 1999 Rq36: Spectroscopy from 0.4 to 2.4 μm and Meteorite Analogs. *Icarus* 216: 462–475.

Clark, B. E., Sen, A., Zou, X. D., DN, D. G., Sugita, S., Sakatani, N., Thompson, M., et al. 2023. Overview of the Search for Signs of Space Weathering on the Low-Albedo Asteroid (101955) Bennu. *Icarus* 400: 115563. https://doi.org/10.1016/j.icarus.2023.115563.

Connolly, H. C., Jr., Lauretta, D. S., McCoy, T. J., Russell, S. S., Haenecour, P., Polit, A., Barnes, J. J., et al. 2025. An Overview of the Petrography and Petrology of Particles from Aggregate Sample from Asteroid Bennu. *Meteoritics & Planetary Science* 60: 979–996. https://doi.org/10.1111/maps.14335.

Delbó, M., Delloro, A., Harris, A., Mottola, S., and Mueller, M. 2007. Thermal Inertia of near-Earth Asteroids and Implications for the Magnitude of the Yarkovsky Effect. *Icarus* 190: 236–249. https://doi.org/10.1016/j.icarus.2007.03.007.

DellaGiustina, D. N., Burke, K. N., Walsh, K. J., Smith, P. H., Golish, D. R., Bierhaus, E. B., Ballouz, R. L., et al. 2020. Variations in Color and Reflectance on the Surface of Asteroid (101955) Bennu. *Science* 370: eabc3660. https://doi.org/10.1126/science.abc3660.

DellaGiustina, D. N., Kaplan, H. H., Simon, A. A., Bottke, W. F., Avdellidou, C., Delbo, M., Ballouz, R. L., et al. 2021. Exogenic Basalt on Asteroid (101955) Bennu. *Nature Astronomy* 5: 31–38. https://doi.org/10.1038/s41550-020-1195-z.

DeMeo, F., Binzel, R. P., Slivan, S. M., and Bus, S. J. 2009. An Extension of the Bus Asteroid Taxonomy into the Near-Infrared. *Icarus* 202: 160–180.

Deshapriya, J. D. P., Barucci, M. A., Bierhaus, E. B., Fornasier, S., Hasselmann, P. H., Merlin, F., Clark, B. E., et al. 2021. Spectral Analysis of Craters on (101955) Bennu. *Icarus* 357: 114252. https://doi.org/10.1016/j.icarus.2020.114252.

Eckley, S. A., Lunning, N. G., O'Neal, E. W., Plummer, J., Funk, R. C., Calva, C., Ferdous, J., et al. 2025. Pristine X-Ray Computed Tomography Imaging of Stones Returned from Asteroid Bennu. In *Workshop on Bennu and Ryugu: Samples from the Early Solar System*. Abstract #2018. https://www.hou.usra.edu/meetings/bennuryugu2025/pdf/2018.pdf.

Gaffey, M. J. 1986. Spectral Reflectance of Carbonate Minerals in the Visible and Near Infrared (0.35–2.55 Microns); Calcite, Aragonite, and Dolomite. *American Mineralogist* 71: 151–162.

Glavin, D. P., Dworkin, J. P., Alexander, C. M. O'D., Aponte, J. C., Baczynski, A. A., Barnes, J. J., Bechtel, H. A., et al. 2025. Abundant Ammonia and Nitrogen-Rich Soluble Organic Matter in Samples from Asteroid (101955) Bennu. *Nature Astronomy* 9: 199–210. https://doi.org/10.1038/s41550-024-02472-9.

Golish, D. R., DellaGiustina, D. N., Li, J. Y., Clark, B. E., Zou, X. D., Smith, P. H., Rizos, J. L., et al. 2021. Disk-Resolved Photometric Modeling and Properties of Asteroid (101955) Bennu. *Icarus* 357: 113724. https://doi.org/10.1016/j.icarus.2020.113724.

Golish, D. R., Shultz, N. K., Becker, T. L., Becker, K. J., Edmundson, K. L., DellaGiustina, D. N., Drouet d'Aubigny, C., et al. 2021. A High-Resolution Normal Albedo Map of Asteroid (101955) Bennu. *Icarus* 355: 114133. https://doi.org/10.1016/j.icarus.2020.114133.

Goodrich, C. A., Lee, S., Mane, P., Hamilton, V. E., Zolensky, M. E., Kita, N. T., Harrington, R., and Jercinovic, M. J. 2023. Ryugu and the Quest for Unaltered CI-Like Materials from the Early Solar System. *Lunar and Planetary Science* LIV: 1446.

Hamilton, V. E., Christensen, P. R., Kaplan, H. H., Haberle, C. W., Rogers, A. D., Glotch, T. D., Breitenfeld, L. B., et al. 2021. Evidence for Limited Compositional and Particle Size Variation on Asteroid (101955) Bennu from Thermal Infrared Spectroscopy. *Astronomy and Astrophysics* 650: A120.

Hamilton, V. E., Haberle, C. W., and Mayerhöfer, T. G. 2020. Effects of Small Crystallite Size on the Thermal Infrared (Vibrational) Spectra of Minerals. *American Mineralogist* 105: 1756–60. https://doi.org/10.2138/am-2020-7602.

Hamilton, V. E., Kaplan, H. H., Connolly, H. C., Goodrich, C. A., Abreu, N. M., and Simon, A. A. 2022. Gro 95577 (Cr1) as a Mineralogical Analogue for Asteroid (101955) Bennu. *Icarus* 383: 115054. https://doi.org/10.1016/j.icarus.2022.115054.

Hamilton, V. E., Simon, A. A., Christensen, P. R., Reuter, D. C., Clark, B. E., Barucci, M. A., Bowles, N. E., et al. 2019. Evidence for Widespread Hydrated Minerals on Asteroid (101955) Bennu. *Nature Astronomy* 3: 332–340. https://doi.org/10.1038/s41550-019-0722-2.

Hanna, R. D., Hamilton, V. E., Haberle, C. H., Kaplan, H. H., Lantz, C., Christensen, P. R., Simon, A. A., and Reuter, D. C. 2023. Phyllosilicate Decomposition on Bennu Due to Prolonged Surface Exposure. *Icarus* 408: 115809. https://doi.org/10.1016/j.icarus.2023.115809.

Hapke, B. 2001. Space Weathering from Mercury to the Asteroid Belt. *Journal of Geophysical Research* 106: 10039–73.

Harrington, R., Lunning, N., and Davidson, J. 2025. Polished Sample Preparation without Liquids. In *Workshop on Bennu and Ryugu: Samples from the Early Solar System*: 2050. https://app.readcube.com/library/8ef6d530-5a2a-4a35-8e29-cd7ec52515c7/item/d8508fe1-b8af-48f7-af87-b53c22067ede.

Henderson, B. G., and Jakosky, B. M. 1997. Near-Surface Thermal Gradients and Mid-Ir Emission Spectra: A New Model Including Scattering and Application to Real Data. *Journal of Geophysical Research* 102(E3): 6567–80.

Hiroi, T., Milliken, R. E., Robertson, K. M., Schultz, C. D., Amano, K., Nakamura, T., Yurimoto, H., et al. 2023. Evidence of Global Space Weathering by Solar Wind on Asteroid 162173 Ryugu. *Icarus* 406: 115755. https://doi.org/10.1016/j.icarus.2023.115755.

Jawin, E. R., Ballouz, R.-L., Ryan, A. J., Kaplan, H. H., McCoy, T. J., al Asad, M. M., Molaro, J. L., Rozitis, B., and Keller, L. P. 2023. Boulder Diversity in the Nightingale Region of Asteroid (101955) Bennu and Predictions for Physical Properties of the Osiris-rex Sample. *Journal of Geophysical Research: Planets* 128: e2023JE008019. https://doi.org/10.1029/2023JE008019.

Jawin, E. R., McCoy, T. J., Walsh, K. J., Connolly, H. C., Jr., Ballouz, R. L., Ryan, A. J., Kaplan, H. H., et al. 2022. Global Geologic Map of Asteroid (101955) Bennu Indicates Heterogeneous Resurfacing in the Past 500,000 Years. *Icarus* 381: 114992. https://doi.org/10.1016/j.icarus.2022.114992.

Kaplan, H. H., Lauretta, D. S., Simon, A. A., Hamilton, V. E., DellaGiustina, D., Golish, D. R., Reuter, D. C., et al. 2020. Bright Carbonate Veins on Asteroid (101955) Bennu: Implications for Aqueous Alteration History. *Science* 370: eabc3557. https://doi.org/10.1126/science.abc3557.

Keller, L. P., Thompson, M. S., Seifert, L. B., Melendez, L. E., Thomas-Keprta, K. L., le, L., Snead, C. J., et al. 2025. Space Weathering Effects Recorded in Bennu Samples. *Nature Geoscience* 18: 825–831. https://doi.org/10.1038/s41561-025-01745-w.

Kitazato, K., Milliken, R. E., Iwata, T., Abe, M., Ohtake, M., Matsuura, S., Arai, T., et al. 2019. Surface Composition of Asteroid 162173 Ryugu as Observed by the Hayabusa2 Nirs3 Instrument. *Science* 364: 272–75.

Klima, R. L., and Pieters, C. M. 2006. Near- and Mid-Infrared Microspectroscopy of the Ronda Peridotite. *Journal of Geophysical Research* 111: E01005. https://doi.org/10.1029/2005JE002537.

Lane, M. D., and Christensen, P. R. 1997. Thermal Infrared Emission Spectroscopy of Anhydrous Carbonates. *Journal of Geophysical Research* 102(E11): 25581–92.

Lantz, C., Brunetto, R., Barucci, M. A., Fornasier, S., Baklouti, D., Bourçois, J., and Godard, M. 2017. Ion Irradiation of Carbonaceous Chondrites: A New View of Space Weathering on Primitive Asteroids. *Icarus* 285: 43–57.

Lauretta, D. S., Adam, C. D., Allen, A. J., Ballouz, R. L., Barnouin, O. S., Becker, K. J., Becker, T., et al. 2022. Spacecraft Sample Collection and Subsurface Excavation of Asteroid (101955) Bennu. *Science* 2022: eabm1018. https://doi.org/10.1126/science.abm1018.

Lauretta, D. S., Bartels, A. E., Barucci, M. A., Bierhaus, E. B., Binzel, R. P., Bottke, W. F., Campins, H., et al. 2015. The Osiris-rex Target Asteroid (101955) Bennu: Constraints on its Physical, Geological, and Dynamical Nature from Astronomical Observations. *Meteoritics & Planetary Science* 50: 834–849. https://doi.org/10.1111/maps.12353.

Lauretta, D. S., Connolly, H. C., Jr., Grossman, J. N., Polit, A. T., and Osiris-REx Sample Analysis Team. 2023. Osiris-Rex Sample Analysis Plan—Revision 3.0. *arXiv*. https://doi.org/10.48550/arxiv.2308.11794.

Lauretta, D. S., DellaGiustina, D. N., Bennett, C. A., Golish, D. R., Becker, K. J., Balram-Knutson, S. S., Barnouin, O. S., et al. 2019. The Unexpected Surface of Asteroid (101955) Bennu. *Nature* 568: 55–60. https://doi.org/10.1038/s41586-019-1033-6.

Lauretta, D. S., Harold, C., Connolly, H. C., Jr., Aebersold, J. E., Alexander, C. M. O'D., Ballouz, R. L., Barnes, J. J., et al. 2024. Asteroid (101955) Bennu in the Laboratory: Properties of the Sample Collected by Osiris-rex. *Meteoritics & Planetary Science* 59: 2453–86. https://doi.org/10.1111/maps.14227.

Levison, H. F., Olkin, C. B., Noll, K. S., Marchi, S., Bell III, J. F., Bierhaus, E., Binzel, R., et al. 2021. Lucy Mission to the Trojan Asteroids: Science Goals. *The Planetary Science Journal* 2: 171. https://doi.org/10.3847/psj/abf840.

Licandro, J., Campins, H., Mothé-Diniz, T., Pinilla-Alonso, N., and de León, J. 2007. The Nature of Comet-Asteroid Transition Object (3200) Phaethon. *Astronomy and Astrophysics* 461: 751–57.

Loeffler, M. J., and Prince, B. S. 2022. A Possible Explanation for the Blue Spectral Slope Observed on B-Type Asteroids. *Icarus* 376: 114881. https://doi.org/10.1016/j.icarus.2022.114881.

Logan, L. M., and Hunt, G. R. 1970. Emission Spectra of Particulate Silicates under Simulated Lunar Conditions. *Journal of Geophysical Research* 75: 6539–48.

Lunning, N. G., and Davidson, J. 2025. X-Ray Computed Tomography Scanning of Nasa Pristine Bennu Samples: Collection Preservation and Selection Process. In *Workshop on Bennu and Ryugu: Samples from the Early Solar System*: 2004. https://app.readcube.com/library/8ef6d530-5a2a-4a35-8e29-cd7ec52515c7/item/489da2dd-89f3-4d7d-92bb-28c0d668e143.

Matrajt, G., Muñoz Caro, G. M., Dartois, E., D'Hendecourt, L., Deboffle, D., and Borg, J. 2005. Ftir Analysis of the Organics in Idps: Comparison with the Ir Spectra of the Diffuse Interstellar Medium. *Astronomy and Astrophysics* 433: 979–995. https://doi.org/10.1051/0004-6361:20041605.

McCoy, T. J., Russell, S. S., Zega, T. J., Thomas-Keprta, K. L., Singerling, S. A., Brenker, F. E., Timms, N. E., et al. 2025. An Evaporite Sequence from Ancient Brine Recorded in Bennu Samples. *Nature* 637: 1072–77. https://doi.org/10.1038/s41586-024-08495-6.

Nakamura, T., Matsumoto, M., Amano, K., Enokido, Y., Zolensky, M. E., Mikouchi, T., Genda, H., et al. 2022. Formation and Evolution of Carbonaceous Asteroid Ryugu: Direct Evidence from Returned Samples. *Science* 379: eabn8671. https://doi.org/10.1126/science.abn8671.

Noguchi, T., Matsumoto, T., Miyake, A., Igami, Y., Haruta, M., Saito, H., Hata, S., et al. 2022. A Dehydrated Space-Weathered Skin Cloaking the Hydrated Interior of Ryugu. *Nature Astronomy* 7: 1–12. https://doi.org/10.1038/s41550-022-01841-6.

Pieters, C. M., Taylor, L. A., Noble, S. K., Keller, L. P., Hapke, B., Morris, R. V., Allen, C. C., DS, M. K. A. Y., and Wentworth, S. 2000. Space Weathering on Airless Bodies: Resolving a Mystery with Lunar Samples. *Meteoritics & Planetary Science* 35: 1101–7.

Pilorget, C., Baklouti, D., Bibring, J. P., Brunetto, R., Ito, M., Franchi, I., Tomioka, N., et al. 2024. Phosphorus-Rich Grains in Ryugu Samples with Major Biochemical Potential. *Nature Astronomy* 8: 1–7. https://doi.org/10.1038/s41550-024-02366-w.

Praet, A., Barucci, M. A., Clark, B. E., Kaplan, H. H., Simon, A. A., Hamilton, V. E., Emery, J. P., et al. 2021. Hydrogen Abundance Estimation and Distribution on (101955) Bennu. *Icarus* 363: 114427. https://doi.org/10.1016/j.icarus.2021.114427.

Praet, A., Poggiali, G., Barucci, M. A., Clark, B. E., Zou, X. D., Simon, A. A., Kaplan, H. H., Li, J. Y., and Alcaria, C. 2022. Evaluating Possible Spectroscopic Variation of Bennu's Sampling Site. *Monthly Notices of the Royal Astronomical Society* 519: 1464–75. https://doi.org/10.1093/mnras/stac2969.

Reuter, D. C., Simon, A. A., Hair, J., Lunsford, A., Manthripragada, S., Bly, V., Bos, B., et al. 2018. The Osiris-rex Visible and Infrared Spectrometer (Ovirs): Spectral Maps of the Asteroid Bennu. *Space Science Reviews* 214. https://doi.org/10.1007/s11214-018-0482-9.

Rozitis, B., Ryan, A. J., Emery, J. P., Christensen, P. R., Hamilton, V. E., Simon, A. A., Reuter, D. C., et al. 2020. Asteroid (101955) Bennu's Weak Boulders and Thermally Anomalous Equator. *Science Advances* 6. https://doi.org/10.1126/sciadv.abc3699.

Ryan, A. J., Ballouz, R. L., Macke, R. J., Ishizaki, T., Alasli, A., Biele, J., Eckley, S. A., et al. 2026. Low Thermal Inertia of Carbonaceous Asteroid Bennu Driven by Cracks Observed in Returned Samples. *Nature Communications* 17: 2443. https://doi.org/10.1038/s41467-026-68505-1.

Salisbury, J. W., Walter, L. S., Vergo, N., and D'Aria, D. M. 1991. *Infrared (2.1–25 μm) Spectra of Minerals*. Baltimore and London: Johns Hopkins University Press.

Sandford, S. A., Gainsforth, Z., Nuevo, M., Marcus, M. A., Bechtel, H. A., Ogliore, R. C., Jones, C., et al. 2025. Nitrogen- and Oxygen-Rich Organic Material Indicative of Polymerization in Pre-Aqueous Cryochemistry on Bennu's Parent Body. *Nature Astronomy* 9: 1803–11.

Schrader, D. L., Cloutis, E. A., Applin, D. M., Davidson, J., Torrano, Z. A., Foustoukos, D., Alexander, C. M. O'D., et al. 2024. Tarda and Tagish Lake: Samples from the Same Outer Solar System Asteroid and Implications for D- and P-Type Asteroids. *Geochimica et Cosmochimica Acta* 380: 48–70. https://doi.org/10.1016/j.gca.2024.07.007.

Simon, A. A., Kaplan, H. H., Cloutis, E., Hamilton, V. E., Lantz, C., Reuter, D. C., Trang, D., Fornasier, S., Clark, B. E., and Lauretta, D. S. 2020. Weak Spectral Features on (101995) Bennu from the Osiris-Rexvisible and Infrared Spectrometer. *Astronomy & Astrophysics* 644: A148.

Simon, A. A., Kaplan, H. H., Hamilton, V. E., Lauretta, D. S., Campins, H., Emery, J. P., Barucci, M. A., et al. 2020. Widespread Carbon-Bearing Materials on Near-Earth Asteroid (101955) Bennu. *Science* 370: eabc3522. https://doi.org/10.1126/science.abc3522.

Simon, A. A., Reuter, D. C., and Lauretta, D. S. 2021. Derivation of the Final Osiris-rex Ovirs in-Flight Radiometric Calibration. *Journal of Astronomical Telescopes, Instruments, and Systems* 7: 1–8. https://doi.org/10.1117/1.Jatis.7.2.020501.

Takir, D., Emery, J. P., McSween, H. Y., Jr., Hibbitts, C. A., Clark, R. N., Pearson, N., and Wang, A. 2013. Nature and Degree of Aqueous Alteration in Cm and Ci Carbonaceous Chondrites. *Meteoritics & Planetary Science* 48: 1618–37.

Trang, D., Thompson, M. S., Clark, B. E., Kaplan, H. H., Zou, X.-D., Li, J.-Y., Ferrone, S. M., et al. 2021. The Role of Hydrated Minerals and Space Weathering Products in the Bluing of Carbonaceous Asteroids. *The Planetary Science Journal* 2: 68. https://doi.org/10.3847/PSJ/abe76f.

Van Schmus, W. R., and Wood, J. A. 1967. A Chemical-Petrologic Classification for the Chondritic Meteorites. *Geochimica et Cosmochimica Acta* 31: 747–765.

Yang, B., and Jewitt, D. 2010. Identification of Magnetite in B-Type Asteroids. *The Astronomical Journal* 140: 692–98.

Yumoto, K., Tatsumi, E., Kouyama, T., Golish, D. R., Cho, Y., Morota, T., Kameda, S., et al. 2024. Comparison of Optical Spectra between Asteroids Ryugu and Bennu: II. High-Precision Analysis for Space Weathering Trends. *Icarus* 420: 116204. https://doi.org/10.48550/arxiv.2407.05258.

Zega, T. J., McCoy, T. J., Russell, S. S., Keller, L. P., Gainsforth, Z., Singerling, S. A., Manga, V. R., et al. 2025. Mineralogical Evidence for Hydrothermal Alteration of Bennu Samples. *Nature Geoscience* 18: 832–39. https://doi.org/10.1038/s41561-025-01741-0.